

Random walkers on a deformable medium

Carlos Lajusticia-Costan,¹ Silvia N. Santalla,² Javier Rodríguez-Laguna,¹ and Elka Korutcheva^{1,3}

¹*Departamento de Física Fundamental, Universidad Nacional de Educación a Distancia (UNED), Madrid, Spain*

²*Departamento de Física and Grupo Interdisciplinar de Sistemas Complejos (GISC),
Universidad Carlos III de Madrid, Madrid, Spain*

³*G. Nadjakov Institute of Solid State Physics, Bulgarian Academy of Sciences, 1784 Sofia, Bulgaria*
(Dated: April 4, 2020)

We consider random walkers that deform the medium as they move, enabling a faster motion in regions which have been recently visited. This induces an effective interaction between walkers mediated by the medium, which can be regarded as the space metric. This gives rise to a statistical mechanics toy model either for gravity, motion through deformable matter or adaptable geometry. In the strong-deformability regime, we find that diffusion is ruled by the *porous medium equation*, thus yielding subdiffusive behavior of an initially localized cloud of particles, whose global width will grow like $\sigma \sim t^{1/3}$, though the width of each sample will sustain a $t^{1/2}$ growth, which can be accounted for through ergodicity breaking. Indeed, random walkers present strong correlation effects which we explore indirectly through the fluctuations of the center of mass of the cloud.

I. INTRODUCTION

Let us consider random walkers in a forest leaving some trail behind them, which they may come across again at a later time. The walkers may then choose to avoid that trail or, otherwise, be attracted towards it. Thus, the walkers interact with the medium, which will interact with the walkers in its turn. Alternatively, we may consider the walkers to have a memory of past events, changing their behavior appropriately.

Random walkers with a memory, which are also called non-Markovian, have been described thoroughly. Specially interesting is the *elephant random walk* (ERW), in which the random walker copies the step taken some random time ago [1–5]. Random walkers can be interpreted as foragers gathering food, and in that case they may decide from time to time to jump to a previous point in their search path, where they were specially successful. This gives rise to the *random walks with relocation* [6–8], which are very useful to describe animal motion, and to develop search algorithms [9, 10].

Self-avoiding walks, on the other hand, were developed in the context of polymer science [11]. The walk is assigned a probability globally, not step-by-step, which becomes zero when the walk intersects itself [12]. Alternatively, random walkers can be either forbidden to cross their previous path, thus allowing them to become trapped, or they may receive an energy penalty for each self-cross [13, 14].

Yet, random walkers may present an affinity towards already visited sites, as it is the case with *taxis* in biology [15, 16], forming *reinforced random-walks* where the walker finds it more likely to step on an already visited site, with memory sometimes fading with time, often to the extreme of only remembering the last step [17–20]. Random walkers may also create a potential well around the visited sites, thus energetically encouraging future visits [21, 22]. Similar ideas have been successfully applied to the design of optimization algorithms on complex landscapes, such as the *ant colony optimization*[23] or the

river formation heuristics[24].

In this work we consider random walkers that reduce the *waiting time* associated with a link each time they traverse it [25–27]. This can be considered equivalent to a change in the local speed of light or, in other words, a deformation in the space-time metric. Thus, walkers move faster in regions which have been recently visited. Yet, we will consider the metric to present a tendency to return to its undeformed state when the walkers are not disturbing it. Thus, our work connects naturally with the problem of diffusion on curved space-times [28] and in relativistic setups [29].

In the continuum limit, these position-dependent waiting times map to an inhomogeneous diffusivity. Thus, we can write down a generalized Fokker-Planck equation with two fields: *matter* is described by the probability distribution for the walker positions, and the *medium* or *geometry* is described by the diffusivity field. The associated partial differential equations are non-linear, and in the strong coupling limit we will show that they are ruled by the *porous medium equation* [30], with non-trivial scaling exponents showing subdiffusive behavior.

This article is organized as follows. Section II describes our discrete 1D random-walk model on a deformable medium (RWDM). The continuum limit of this model is considered in Sec. III, which discusses the expected scaling properties. Extensive numerical simulations are performed and discussed in Sec. IV, which give rise to a physical picture which is discussed in Sec. V. Finally, Sec. VI provides a summary of the conclusions and proposals for further work.

II. RANDOM-WALK ON DEFORMABLE MEDIUM

Let us describe our model, which will be called the *random walk on a deformable medium* (RWDM) and where we consider N_P random walkers on a chain. When a walker is standing on site i , it has a certain probability

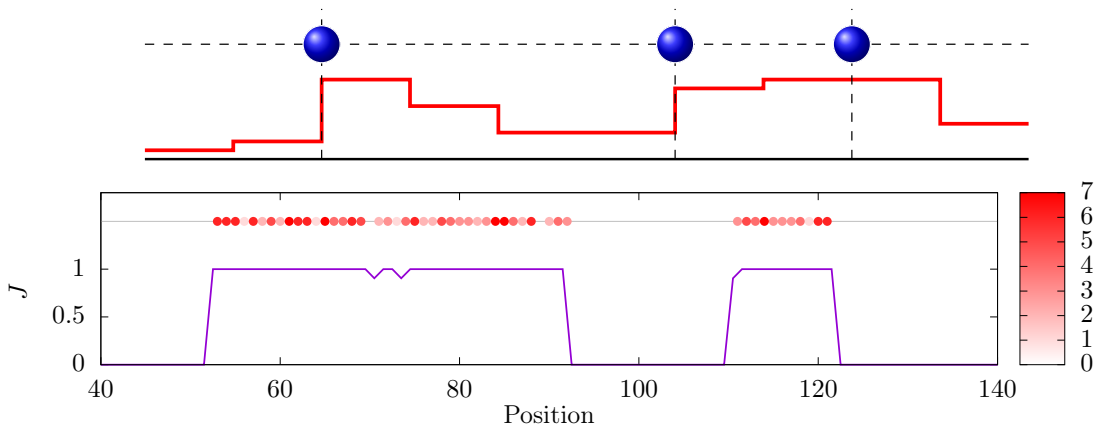


Figure 1. Top: Illustration of the RWDM model. Walkers occupy integer positions of a chain, and hopping probabilities between neighboring sites can be different. Bottom: A configuration for $\mathcal{J}_0 = 10^{-6}$, $\mathcal{J}_1 = 1$, $t_0 = 10$ and $N_P = 100$ particles on $L = 200$ sites, after $T = 10^8$ time-steps. The purple line denotes the hopping probabilities, red balls represent the positions of the particles, and the color intensity denotes the number of particles at a certain site. Notice that most hopping probabilities are near \mathcal{J}_0 or \mathcal{J}_1 , and that the particles are neatly divided into two blocks.

per unit time $J_{i,i-1}$ of hopping towards site $i - 1$, and $J_{i,i+1}$ of hopping towards site $i + 1$. We will assume that these probabilities are symmetric, i.e. $J_{i,i+1} = J_{i+1,i}$, and we will introduce the convenient notation $J_i \equiv J_{i,i+1}$. Notice that the hopping process on a single link follows a Poissonian law, and that the expected *waiting time* before hopping is $\tau = J^{-1}$. The walker may take either its left link with hopping rate J_{i-1} or its right link with hopping rate J_i . Fig. 1 provides an illustration of our basic model.

The system starts with uniform hopping rates, $J_i = \mathcal{J}_0$ for all i . Whenever the particle hops across link $(i, i + 1)$, the hopping probability is updated, $J_i = \mathcal{J}_1 \geq \mathcal{J}_0$. Thus, a link that has just been crossed presents a lower waiting time, making it easier to revisit. Yet, we will introduce another element: *link relaxation*. If the link has not been used, it decays exponentially towards its undeformed value, \mathcal{J}_0 , with a characteristic time t_0 .

We have developed a numerical simulation scheme for RWDM systems, in which N_P particles are initially placed at the center of a size L chain with periodic boundaries with all hopping probabilities $J_i = \mathcal{J}_0$. A suitable time-step is chosen, Δt . At each turn, we select a random particle and look up its location, i . Also, we decide to attempt a jump to the left or to the right with equal probabilities. The jump attempt will succeed with probability $P = J_k \Delta t$, where $k = i - 1$ for a left jump, or $k = i$ for a right jump. After a successful jump attempt, the link will increase its hopping probability: $J_k \rightarrow \mathcal{J}_1$, thus completing the turn. After a round of N_P turns, we assert that time has advanced by a time-step Δt . Then, all links which have not been updated during this round are subject to the relaxation rule,

$$J_p \rightarrow J_p - \frac{\Delta t}{t_0} (J_p - \mathcal{J}_0). \quad (1)$$

Notice that, in the continuum limit, this corresponds to an exponential decay towards the relaxed value, with characteristic time t_0 .

If $\mathcal{J}_1 = \mathcal{J}_0$, the metric becomes rigid and the particles will follow a standard random walk. Thus, in this limit we expect that the particle cloud will behave diffusively, i.e. the expected deviation of the particle positions will scale like $\sigma \sim t^{1/2}$. If $\mathcal{J}_1 \geq \mathcal{J}_0$ then the particles will present a trend to hop on already used links, thus spending more time on the regions already visited. This may lead to *self-localization* of the particle cloud, through interaction with the medium. In this case, we may still expect a power-law behavior, with $\langle d(t) \rangle \sim t^\alpha$ and $\alpha < 1/2$.

Fig. 2 shows two histories, using $\Delta t = 1$, $\mathcal{J}_0 = 10^{-6}$ and $\mathcal{J}_1 = 1$ on a $L = 200$ chain with $N_P = 200$ particles. The X-axis represents time in logarithmic scale, while the Y-axis represents the position. Color intensity denotes the hopping probabilities J_i , where we can see that only values close to \mathcal{J}_0 and \mathcal{J}_1 are really present. The width of the cloud at a certain time can be estimated from the vertical range of the high hopping region, $\mathcal{H} \equiv \{i | J_i \approx \mathcal{J}_1\}$. Indeed, the cloud stays localized at the center up to times of order $\exp(8) \approx 3000$, increasing initially and then either opening up (top) or shifting laterally (bottom). Two trajectories of individual particles have been traced, showing that the walkers really spread all over the high-hopping region.

III. CONTINUUM DESCRIPTION

In order to determine the macroscopic behavior of our model, we will assume that matter can be described through a density function, $P(x, t)$, such that the expected number of particles in a region \mathcal{A} will be given by

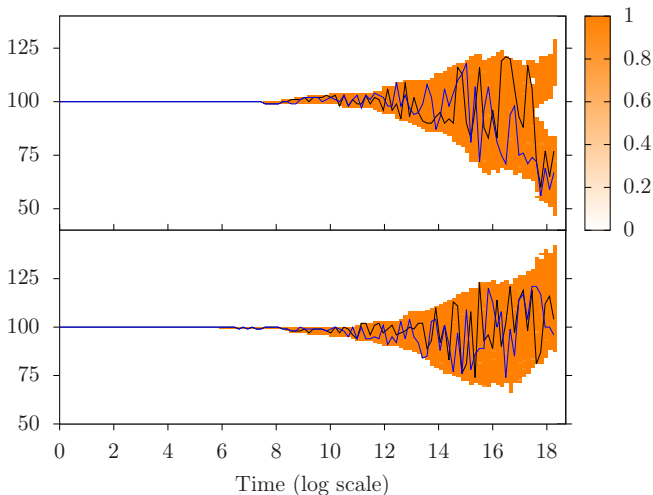


Figure 2. Two system histories, using $N_P = 200$ particles, $\mathcal{J}_0 = 10^{-6}$, $\mathcal{J}_1 = 1$, and $L = 200$. Time is represented in the horizontal axis, in logarithmic scale, while the Y-axis stands for positions along the chain. Color denotes the local hopping probability, and two particle histories (out of $N_P = 200$) are depicted with continuous lines.

$$\langle N_{\mathcal{A}}(t) \rangle = N_P \int_{\mathcal{A}} dx P(x, t). \quad (2)$$

Density correlations are neglected and the function $P(x, t)$ will be assumed to be smooth. Moreover, the hopping terms will be described by a smooth function too, $J(x, t)$, which we will call the metric field. The evolution of the density function will be ruled by a Fokker-Planck equation, considering the drift and diffusion terms,

$$\partial_t P(x, t) = \partial_x (J(x, t) \partial_x P(x, t)), \quad (3)$$

which can be understood as a conventional Fokker-Planck equation when the underlying metric has the form

$$ds^2 = -J(x) dt^2 + J(x) dx^2. \quad (4)$$

Making use of the new coordinates

$$\begin{aligned} dx' &= J(x) dx, \\ dt' &= J(x) dt, \end{aligned} \quad (5)$$

and transforming appropriately the operator

$$\partial_t - \partial_x^2, \quad (6)$$

in the limit where the time evolution of $J(x, t)$ is slow we obtain (3) and a flat, Minkowskian line element,

$$ds^2 = -dt'^2 + dx'^2, \quad (7)$$

in a transformed coordinate system, which is the expected result.

Yet, the metric field $J(x, t)$ is not fixed beforehand in our model. Instead, it depends dynamically on the matter field $P(x, t)$, giving rise to a back-reaction of the matter into the metric. Indeed, we may claim that the geometry tells matter how to move through Eq. (3), while matter tells geometry how to curve through an equation that we will derive in the next paragraphs.

In order to determine the evolution equation of the geometry, let us consider the microscopic mechanism. Wherever there are moving particles, the hopping probability increases up to \mathcal{J}_1 , and where there are no particles, the hopping probability decays to \mathcal{J}_0 . Thus, we can propose the following equation

$$\begin{aligned} \partial_t J(x, t) &= K_1 P(x, t) [\mathcal{J}_1 - J(x, t)] \\ &+ K_0 (1 - P(x, t)) [\mathcal{J}_0 - J(x, t)], \end{aligned} \quad (8)$$

where K_1 and K_0 are the increasing and decreasing rates, respectively. In our microscopic model, $K_1 \gg K_0 \approx 1/t_0$, but we will assume them to be identical $K_1 = K_0 = K$. Thus, we can reorganize the terms,

$$\partial_t J(x, t) = K (P(x, t)(\mathcal{J}_1 - \mathcal{J}_0) + \mathcal{J}_0 - J(x, t)). \quad (9)$$

Let us consider the limit of very fast back-reaction between the metric and the matter fields, $K \rightarrow \infty$ or $t_0 \rightarrow 0$. In that limit, the term in parenthesis in Eq. (9) must vanish, and we have

$$J(x, t) = P(x, t)(\mathcal{J}_1 - \mathcal{J}_0) + \mathcal{J}_0, \quad (10)$$

Plugging this equation into our original Fokker-Planck Eq. (3), we can find a non-linear equation for the matter field alone,

$$\partial_t P(x, t) = \Delta \mathcal{J} (\partial_x P(x, t))^2 + [\mathcal{J}_0 + \Delta \mathcal{J} P(x, t)] \partial_x^2 P(x, t), \quad (11)$$

where $\Delta \mathcal{J} \equiv \mathcal{J}_1 - \mathcal{J}_0$. We can also solve for $J(x, t)$, resulting in

$$\partial_t J(x, t) = \partial_x (J(x, t) \partial_x J(x, t)). \quad (12)$$

Furthermore, in the limit in which $\mathcal{J}_0 \rightarrow 0$ and $\Delta \mathcal{J} \rightarrow \mathcal{J}_1$ we reach an effective equation for the matter field,

$$\begin{aligned} \partial_t P(x, t) &= \mathcal{J}_1 ((\partial_x P(x, t))^2 + P(x, t) \partial_x^2 P(x, t)) \\ &= \frac{\mathcal{J}_1}{2} \partial_x^2 (P^2(x, t)). \end{aligned} \quad (13)$$

This last equation is a parabolic partial differential equation known as the *porous medium equation* (PME) [30], which is a non-linear relative of the heat equation.

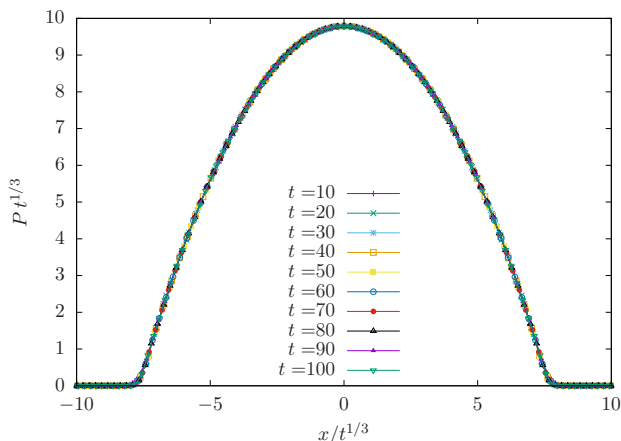


Figure 3. Rescaled solutions of the porous medium equation, Eq. (13) with a Dirac delta function as the initial condition, showing the collapse predicted in Eq. (14).

Opposite to the heat equation, the PME is *causal*, presenting a well-defined light-cone. Also, the scaling properties are very different from the heat equation. Indeed, it has solutions of the form

$$P(x, t) = t^{-\alpha} P(xt^{-\beta}, 1) = t^{-\alpha} F(\eta), \quad (14)$$

where $\eta = xt^{-\beta}$, $\alpha = \beta = 1/3$ and F is a universal function. We have checked numerically the validity of Eq. (14) in Fig. 3. In order to perform the check, we have obtained numerically the solution of the PME, Eq. (13), with a Dirac delta function as the initial condition, $P(x, 0) = \delta(x)$. The solution is suitably rescaled, showing $t^\alpha P(x, t)$ as a function of $xt^{-\beta}$ for several values of t . The different curves collapse into the universal function F , as predicted.

Note that this theoretical framework suggests that the spread of the particle cloud will grow sub-diffusively, $\sigma \sim t^{1/3}$. In the following section, we will discuss the validity of this prediction.

IV. NUMERICAL SIMULATIONS

We have considered an $L = 200$ chain with periodic boundaries, using $N_P = 25, 50, 100$ and 200 particles, with $\mathcal{J}_0 = 10^{-6}$, $\mathcal{J}_1 = 1$, $t_0 = 10$ and $\Delta t = 1$, similarly to the two histories shown in Fig. 2. In all cases, we have simulated up to time $T_{\max} = 10^8$, taking $N_S = 1000$ samples. Throughout this section we define $x_{p,s}(t)$ as the position of particle p in sample s at time t , and $J_i(t; s)$ as the hopping probability between sites i and $i + 1$ in sample s at time t . The initial condition is given by

$$x_{p,s}(0) = L/2, \quad \text{for all } p \text{ and } s, \quad (15)$$

$$J_{i,s}(0) = \mathcal{J}_0, \quad \text{for all } i \text{ and } s. \quad (16)$$

We must make a distinction between averaging over particles, $E_P[\cdot]$, averaging over samples, $E_S[\cdot]$, and averaging over both simultaneously, $E_{SP}[\cdot]$, defined as

$$E_S[X_s] \equiv \frac{1}{N_S} \sum_{s=1}^{N_S} X_s, \quad (17)$$

$$E_P[X_p] \equiv \frac{1}{N_P} \sum_{p=1}^{N_P} X_p, \quad (18)$$

$$E_{SP}[X_{p,s}] \equiv E_S[E_P[X_{p,s}]] = E_P[E_S[x_{p,s}]], \quad (19)$$

and the corresponding variances, $\sigma_{\mathcal{O}}^2[X] = E_{\mathcal{O}}[X^2] - E_{\mathcal{O}}[X]^2$, for $\mathcal{O} \in \{S, P, SP\}$. Alternatively, we can consider E_S to be an expectation value over the full configuration space, i.e.: averaging over all replicas, if replica symmetry is broken.

In Fig. 4 we have considered the evolution of the average size, or width, of the particle cloud, defined in two alternative ways. In the top panel of Fig. 4 we have measured that width as

$$W_{\text{all}}^2(t) = \sigma_{SP}^2[x_{p,s}(t)], \quad (20)$$

which can be compared with the average value of the widths of each sample, shown in the central panel of Fig. 4, which is defined as

$$W_{\text{av}}^2(t) = E_S[\sigma_P^2[x_{p,s}(t)]]. \quad (21)$$

Necessarily, the deviation of the whole ensemble of particle positions must exceed (or be equal to) the average of the deviations within each sample,

$$W_{\text{all}}^2(t) \geq W_{\text{av}}^2(t). \quad (22)$$

For both definitions we can see that the width grows approximately as a power-law for a range of times, and both curves collapse when the time and width axes are rescaled dividing by the number of particles N_P . Interestingly, there are also notable differences between both definitions of width of the cloud. Indeed, the approximate exponents differ, while $W_{\text{all}} \sim t^{1/3}$, we can see that $W_{\text{av}} \sim t^{1/2}$. Yet, the scaling behavior of $W_{\text{all}}(t)$ does not behave exactly the same for the different values of N_P . Moreover, W_{av} saturates after a time that scales linearly with N_P , while W_{all} does not. Indeed, W_{all} provides the expected behavior for the width of the particle cloud predicted in by the continuum approximation, provided by the scaling of the PME, Eq. (13), see Eq. (14). The reasons for the strong discrepancy between both measures will be discussed in the next section.

The full histogram for the particle positions, considering all samples simultaneously, is provided in Fig. 5, for different times (exponentially scaled), using two numbers of particles, $N_P = 50$ (top panel) and $N_P = 200$ (center).

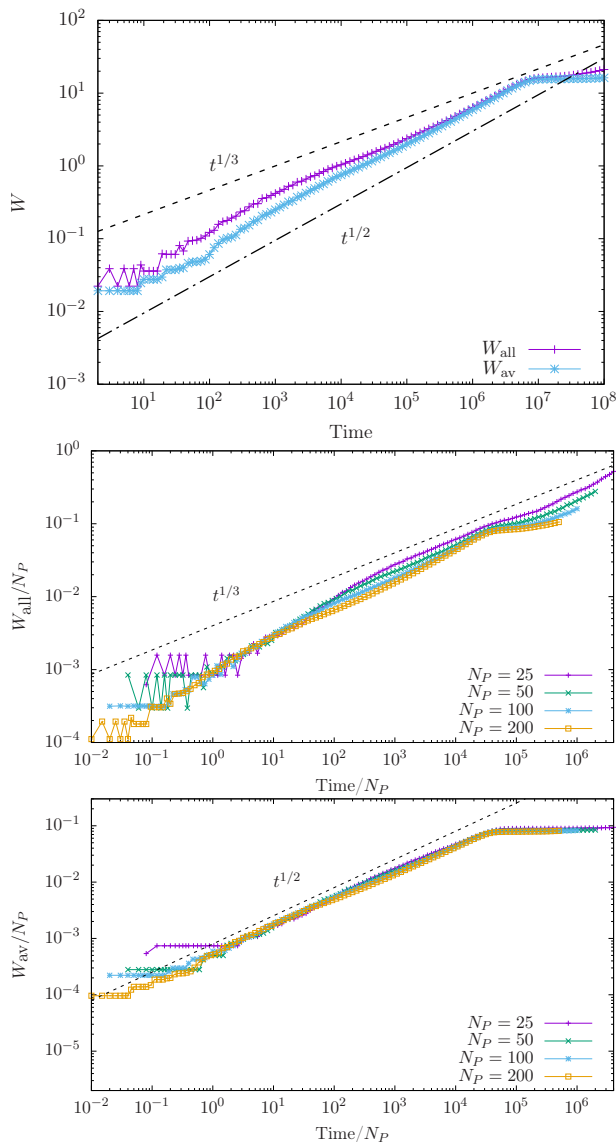


Figure 4. Average width of the particle cloud, as a function of time. Top: comparison of $W_{\text{all}}(t)$, Eq. (20), and $W_{\text{av}}(t)$, Eq. (21), using $N_P = 200$. Notice that inequality (22) holds exactly, saturating in the long run. Center: W_{all} as a function of time, both rescaled with the number of particles N_P , showing the power-law $t^{1/3}$. Bottom: W_{av} as a function of time, rescaled in the same way, while the dashed line represents $t^{1/2}$.

For very short times, the histograms are very peaked, getting wider with time, following the law for $W_{\text{all}}(t)$. Yet, there are substantial differences between the behavior of the histogram for the two different numbers of particles. Indeed, for $N_P = 200$ we observe a flat histogram for intermediate times, which is not so pronounced for $N_P = 50$. Further information can be obtained by measuring the (excess) kurtosis, as shown in the bottom panel of Fig. 5. Indeed, we can observe that, for short times, the distributions are extremely *leptokurtic* (peaked), with the kurtosis decreasing approximately as $\kappa \sim t^{-7/6}$ until

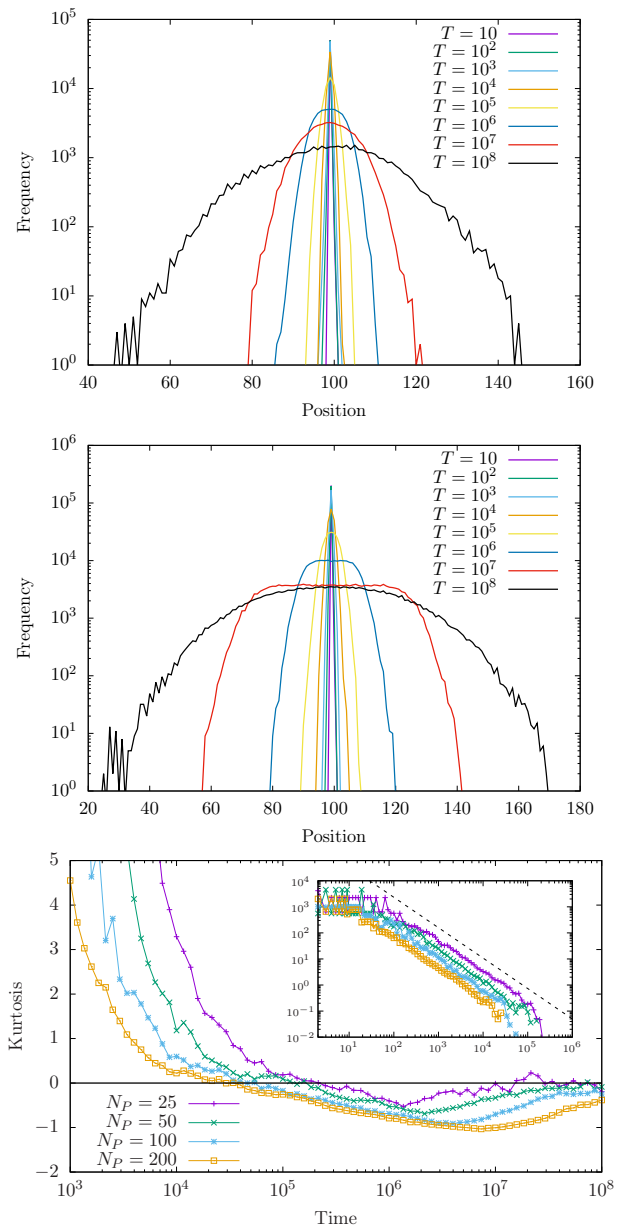


Figure 5. Particle histograms for different times, for $N_P = 50$ (top) and $N_P = 200$ (central), always showing $N_S N_P$ data, with $N_S = 1000$. Notice that broader histograms correspond to later times. Bottom: time evolution of the (excess) kurtosis of the particle histograms for different values of N_P . Inset: log-log plot of the same data, showing a scaling law, $\text{Kurt} \sim t^{-7/6}$.

it becomes negative (platykurtic, square-like) and, then, slowly evolving towards zero, i.e. Gaussian-like.

The size of the cloud can be accessed also through an analysis of the set of hopping probabilities, $\{J_i\}_{i=1}^L$. Let us consider the observable

$$N_J = \frac{1}{\mathcal{J}_1 - \mathcal{J}_0} \sum_{i=1}^L (J_i - \mathcal{J}_0). \quad (23)$$

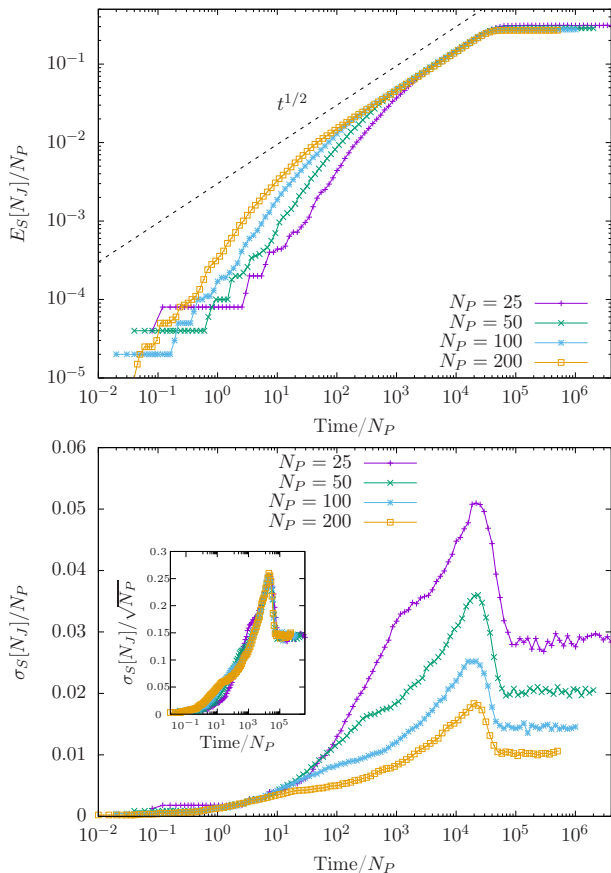


Figure 6. Top: Average number of active hopping probabilities as a function of time, both scaled with the number of particles N_P , compare to Fig. 4 (bottom). The continuous line corresponds to a $t^{1/2}$ scaling. Bottom: sample-to-sample deviation of that magnitude. Inset: scaling with the square root of the number of particles makes the curves collapse.

If all J_i are either \mathcal{J}_0 or \mathcal{J}_1 , N_J measures the number of \mathcal{J}_1 values. Fig. 6 (top) represents the expected value, $E_S[N_J]$, scaled with the number of particles N_P , as a function of time, also divided by N_P . We observe a similar behavior to $W_{\text{av}}(t)$, with a time range with $t^{1/2}$ scaling followed by saturation.

We may ask about the fluctuations in the size of the particle cloud, by measuring $\sigma_S[N_J]$, which appears in the bottom panel of Fig. 6. In this case, the curves for different N_P do not collapse unless we scale differently the time axis (dividing by N_P) and $\sigma_S[N_J]$, which should be divided by $N_P^{1/2}$, as we show in the inset. We observe a steady increase of $\sigma_S[N_J]$ with time, followed by a quick decay at the saturation time towards a constant value.

In order to complete the physical picture, which is described in Sec. V, we have also considered the fluctuations of the center of mass (CM) of the particle cloud. Indeed, for every time and sample we can define

$$X_{CM,s}(t) \equiv E_P[x_{p,s}(t)], \quad (24)$$

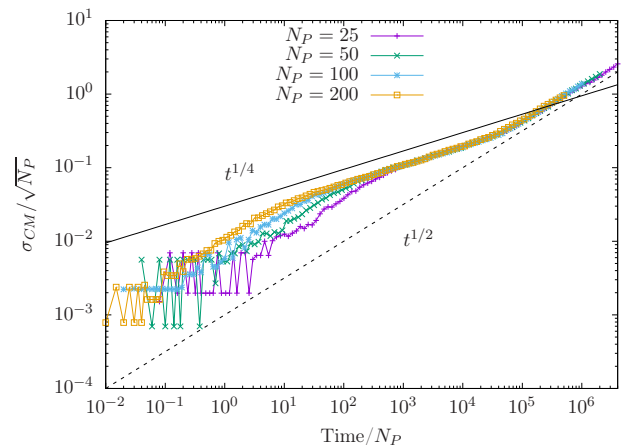


Figure 7. Fluctuations of the center of mass of the particle clouds, for different numbers of particles. The straight lines represent $t^{1/4}$ (continuous line) and $t^{1/2}$ (dashed line).

and we can define the fluctuations over the samples of this magnitude,

$$\sigma_{CM}^2(t) \equiv \sigma_S^2[E_P[x_{p,s}(t)]], \quad (25)$$

The behavior of $\sigma_{CM}(t)$ is shown in Fig. 7 for different numbers of particles, where this time we have rescaled differently, $\sigma_{CM}/N_P^{1/2}$ as a function of time divided by N_P . We observe an intermediate regime where the fluctuations of the center of mass scale as $t^{1/4}$, followed by a long-term diffusive scaling with $t^{1/2}$.

The sample-to-sample fluctuations of the CM position are strongly tied to the difference between W_{all} and W_{av} expressed in inequality (22). Indeed,

$$W_{\text{all}}^2 - W_{\text{av}}^2 = E_S[E_P[x_{p,s}]^2] - E_S[E_P[x_{p,s}]]^2 = \sigma_{CM}^2, \quad (26)$$

i.e. they correspond to the distance between both curves in Fig. 4 (top), see inequality (22).

V. PHYSICAL PICTURE

The numerical data described in the previous section allow us to provide a physical picture for the statistical properties of the cloud of random walkers and the metric field in the RWDM model, based on *broken ergodicity*, i.e., the time evolution of each sample differs from the ensemble evolution. The most salient evidence is the remarkable difference between W_{all} and W_{av} , check Fig. 4.

The physical reason behind this broken ergodicity is the noise amplification at early stages. When the evolution starts, all the particles are concentrated at the center waiting to hop on a \mathcal{J}_0 link, which will take a time $\sim \mathcal{J}_0^{-1}$. The first particle taking such a hop will make all the other particles follow, and the particle cloud as a whole will start hopping between two neighboring sites

for a while, until a second particle hops on a new \mathcal{J}_0 link again, thus spreading the cloud. Notice that different samples will make different choices during these initial steps. Thus, the *average width* of each cloud becomes much smaller than the global width of the ensemble of all clouds. Yet, they grow at different rates: each cloud grows diffusively, with $t^{1/2}$, see Fig. 4, while the global cloud grows subdiffusively, approximately with $t^{1/3}$, which corresponds to the global behavior of the solution of the PME, see Eq. (13) and (14).

As the cloud expands, all internal links are close to their high value, \mathcal{J}_1 . Thus, our estimate of the number of active links, N_J , defined as in (23) and shown in Fig. 6, presents the same scaling as the average width of the clouds, W_{av} , as shown in the central panel of Fig. 4. Yet, the clouds can not expand without limit. The number of particles is finite, so the number of active links that they can occupy grows linearly with N_P . Hence the saturation value both for W_{av} and N_J . Furthermore, when the width of the cloud grows too much, there is a finite probability that some links will not be occupied in a time $> t_0$, thus allowing them to return to their low value, \mathcal{J}_0 , as we can check in Fig. 2. The evolution of the kurtosis of the histograms, Fig. 5 (bottom) points in the same direction: the histograms become *platykurtic* (negative kurtosis, square-like) during the growth regime, tending slowly towards a Gaussian.

The sample-to-sample fluctuations of the CM of the clouds are also very informative, see Fig. 7. Indeed, before saturation the deviation $\sigma_{CM} \sim t^{1/4}$ grows subdiffusively. Beyond saturation, the cloud does not expand any more, and its fluctuations are therefore diffusive.

VI. CONCLUSIONS AND FURTHER WORK

We have considered a model of *random walkers on a deformable medium* (RWDM), an model in which random walkers interact with the medium on which they move. Indeed, the hopping probability associated to each link becomes a dynamical variable, which gets higher when it is actually used, or relaxes towards a lower equilibrium value otherwise. The reinforcement of actually used paths presents similarities with neural plasticity: *neurons that fire together wire together*, also known as Hebb's rule [31]. Adaptable networks appear in a variety of settings, where usage of a link tends to reinforce

its strength and, thus, the probability of further usage [32, 33]. Moreover, the RWDM can also serve as a toy model of stochastic gravity since the medium can be considered as a (1+1)D metric, following the rule that matter tells geometry how to curve and geometry tells matter how to move.

For the sake of concreteness, we have focused on the 1D case, starting with an initial condition in which all particles are concentrated at the center, and the medium starts relaxed, in the limit in which the excited hopping is much larger than the equilibrium one, and for fast relaxation. In that limit, a continuum description should be provided by the *porous medium equation* (PME), which presents scaling solutions in this regime: our cloud should expand subdiffusively with time, due to self-localization effects, and grow like $\sim t^{1/3}$.

Indeed, this subdiffusive growth is observed in numerical experiments, but only when we consider the global cloud consisting of all samples, i.e. an average over the whole configuration space. On the other hand, when we consider the average over samples of the width of *each* cloud, we observe a diffusive behavior, $t^{1/2}$. Yet, the global width must necessarily exceed the average width, and their difference is related to the fluctuations of the center of mass of each cloud. Thus, we were able to identify a growth regime and a saturation regime, where the average width saturates, yet the global width still can grow because the center of mass of the cloud can still wander.

Statistical mechanics of the RWDM seems to provide a wealth of behaviors which are worth exploring, since the few-particle effective interaction, extension to several dimensions or spread initial configurations, which can give rise to cluster formation. Moreover, critical behavior on a gravity field has been extensively studied using Liouville theory, giving rise to the well-known Knizhnik-Polyakov-Zamolodchikov (KPZ) equation which evaluates how the critical exponents of a 2D conformal field theory (CFT) deform in presence of gravity [34, 35]. We intend to explore all these connections in the forecoming future.

ACKNOWLEDGMENTS

We would like to thank Rodolfo Cuerno for his help and valuable insights. Also, we acknowledge the Spanish government for financial support through grant PGC2018-094763-B-I00.

-
- [1] So-called because elephants are believed to have long term memory.
 - [2] G.M. Schütz, S. Trimper, *Elephants can always remember: exact long-range memory effects in a non-Markovian random walk*, Phys. Rev. E **70**, 045101(R) (2004).
 - [3] N. Kumar, U. Harbola, K. Lindenberg, *Memory-induced anomalous dynamics: Emergence of diffusion, subdif-*

- fusion, and superdiffusion from a single random walk model*, Phys. Rev. E **82**, 021101 (2010).
- [4] M.A.A. da Silva, G.M. Viswanathan, J.C. Cressoni, *Ultraslow diffusion in an exactly solvable non-Markovian random walk*, Phys. Rev. E **89**, 052110 (2014).
- [5] M.J. Kearney, R.J. Martin, *Random walks exhibiting anomalous diffusion: elephants, urns and the limits of*

- normality, *J. Stat. Mech.* 013209 (2018).
- [6] D. Boyer, J.C.R. Romo-Cruz, *Solvable random-walk model with memory and its relation with Markovian models of anomalous diffusion*, *Phys. Rev. E* **90**, 042136 (2014).
- [7] D. Boyer, C. Solis-Salas, *Random walks with preferential relocations to places visited in the past and their applications to biology*, *Phys. Rev. Lett.* **112**, 240601 (2014).
- [8] D. Boyer, I. Pineda, *Slow Lévy Walks*, *Phys. Rev. E* **93**, 022103 (2016).
- [9] A. Falcón-Cortés, D. Boyer, L. Giuggioli, S.N. Majumdar, *Localization transition induced by learning in random searches*, *Phys. Rev. Lett.* **119**, 140603 (2017).
- [10] D. Campos, V. Méndez, *Phase transitions in optimal search times: how random walkers should combine resetting and flight scales*, *Phys. Rev. E* **92**, 062115 (2015).
- [11] P.-G. de Gennes, *Scaling concepts in polymer physics*, Cornell Univ. Press (1979).
- [12] D.J. Amit, G. Parisi, L. Peliti, *Asymptotic behavior of the "true" self-avoiding walk*, *Phys. Rev. B* **27**, 1635 (1983).
- [13] C. Domb, G.S. Joyce, *Cluster expansion for a polymer chain*, *J. Phys. C: Solid State Phys.* **5**, 956 (1972).
- [14] H.E. Stanley, K. Kang, S. Redner, R.L. Blumberg, *Novel superuniversal behavior of a random walk model*, *Phys. Rev. Lett.* **51**, 1223 (1983).
- [15] R. Permantle, *A survey of random processes with reinforcement*, *Prob. Surveys* **4**, 1 (2007).
- [16] H.G. Othmer, A. Stevens, *Aggregation, blowup and collapse: the ABC's of taxis in reinforced random walks*, *SIAM J. Appl. Math.* **57**, 1044 (1997).
- [17] B. Davis, *Reinforced random walk*, *Probab. Theor. Rel. Fields* **84**, 203 (1990).
- [18] A. Ordemann, E. Tomer, G. Berkolaiko, S. Havlin, A. Bunde, *Structural properties of self-attracting walks*, *Phys. Rev. E*, **64**, 046117 (2001).
- [19] J.G. Foster, P. Grassberger, M. Paczuski, *Reinforced walks in two and three dimensions*, *New J. Phys.* **11**, 023009 (2009).
- [20] V.B. Sapozhnikov, *Self-attracting walk with $\nu < 1/2$* , *J. Phys. A: Math. Gen.* **27**, L151 (1994).
- [21] S.Y. Huang, X.W. Zou, Z.Z. Jin, *Multiparticle random walks on a deformable medium*, *Phys. Rev. E* **66**, 041112 (2002).
- [22] Z.J. Tan, X.W. Zou, S.Y. Huang, W. Zhang, Z.Z. Jin, *Patterns of particle distribution in multiparticle systems by random walks with memory enhancement and decay*, *Phys. Rev. E* **66**, 011101 (2002).
- [23] M. Dorigo, G. di Caro, *Ant colony optimization: A new meta-heuristic*, in Proc. of the 1999 Congress on Evolutionary Computation, CEC 1999, pp. 1470 (1999); M. Dorigo, T. Stützle, *Ant Colony Optimization*, The MIT Press (2004).
- [24] P. Rabanal, I. Rodríguez, F. Rubio, *Using river formation dynamics to design heuristic algorithms*, in International Conference on Unconventional Computation, page 163, Springer (2007); P. Rabanal, I. Rodríguez, F. Rubio, *Applications of river formation dynamics*, *J. Comp. Science* **22**, 26 (2017).
- [25] T. Miyazawa, T. Izuyuma, *Diffusion in one-dimensional inhomogeneous media*, *Phys. Rev. A* **36**, 5791 (1987).
- [26] J.F. Bouchaud, A. Georges, *Anomalous diffusion in disordered media: statistical mechanics, models and physical applications*, *Phys. Rep.* **195**, 127 (1990).
- [27] Y. Li, O. Kahraman, C.A. Haselwandter, *Distribution of randomly diffusing particles in inhomogeneous media*, *Phys. Rev. E* **96**, 032139 (2017).
- [28] M. Smerlak, *Diffusion in curved spacetimes*, *New J. Phys.* **14**, 023019 (2012).
- [29] J. Dunkel, P. Hänggi, *Relativistic Brownian motion*, *Phys. Rep.* **471**, 1 (2009).
- [30] Juan Luis Vazquez, *The Porous Medium equation*, Clarendon Press Oxford (2007).
- [31] J. Hertz, A. Krogh, R.G. Palmer, *Neural computations*, Addison Wesley (1990).
- [32] T. Gross, H. Sayama, *Adaptive networks*, Springer (2009).
- [33] H. Sayama et al., *Modeling complex systems with adaptive networks*, *Comp. & Math. App.* **65**, 1645 (2013).
- [34] V. Knizhnik, A. Polyakov, A. Zamolodchikov, *Fractal structure of 2d quantum gravity*, *Mod. Phys. Lett. A* **3**, 819 (1988).
- [35] J. Ambjørn, K.N. Anagnostopoulos, U. Magnea, G. Thorleifsson, *Geometrical interpretations of the Knizhnik-Polyakov-Zamolodchikov*, *Phys. Lett. B* **388**, 713 (1996).